Direct and Compound-Nucleus Neutrons from 14–18-MeV Protons on ^{9}Be, ^{14}N, ^{27}Al, ^{56}Fe, ^{115}In, ^{181}Ta, and ^{208}Pb and from 33-MeV Bremsstrahlung on ^{27}Al, ^{206}Pb, ^{208}Pb, and ^{209}Bi*

VICTOR V. VERBINSKI† AND WALTER R. BURRUS‡
Oak Ridge National Laboratory, Oak Ridge, Tennessee 37830
(Received 24 June 1968)

The angle-integrated experimental (p,xn) spectra, fitted with precompound and evaporation spectra from Griffin's statistical model of intermediate structure, produced g, the number of independent-particle states per MeV, and f_c, the compound fraction. For ^{27}Al, ^{56}Fe, ^{115}In, and ^{181}Ta, g increased linearly with A, from 2 to 13, but decreased to 9 ± 1 for ^{208}Pb, at 18-MeV proton energy E_p. At $E_p=14$ MeV, $g=7\pm1$ for ^{208}Pb, which may signify vanishing shell effects at large E_p. Monte Carlo-type intranuclear-cascade-plus-evaporation calculations yielded spectra and cross sections in agreement with the measurements, allowing for several calculational defects that were made obvious in the comparisons. The Monte Carlo calculations yielded f_c values close to those derived by fitting the data with Griffin's calculations for targets heavier than ^{27}Al. "Nuclear temperatures," obtained from LeCouteur's evaporation analysis for multiple-nucleon emissions, agreed for (p,xn) and giant-resonance (γ,xn) reactions, both via the intermediate nucleus ^{209}Bi, but differed considerably for the target ^{27}Al, where direct and evaporation neutrons are not well separated in mean energy. The three types of analyses utilized here are therefore much more applicable for heavy nuclei than for light. Energy and angle dependence of (γ,xn) reactions indicate negligible direct effects, in sharp contrast to (p,xn) reactions, which display a strong forward anisotropy at the high-energy end of the spectra.

I. INTRODUCTION

MEASUREMENTS of neutron spectra were made with moderately poor energy resolution for (p,xn) reactions. These were further smoothed by integration over angle and converted to energy-differential neutron production cross sections. This type of data is suitable for evaluating the three types of calculations referred to below. These calculations are all structureless in terms of well-known variations along the periodic table, so that such effects as may be due to shell structure, collective states, and other types of variation with A could be expected to show up in these comparisons.

The neutron spectra measured at a few angles for (γ,xn) reactions produced by 33-MeV end point bremsstrahlung irradiation were found to be smooth in spite of the fact that the giant dipole resonance selects a relatively narrow band of energy from the broad bremsstrahlung spectrum.[1] The backward-angle spectra were compared with the angle-integrated (p,xn) spectra, referred to as (p,n) spectra below. This comparison is of interest because the low-energy evaporation component is expected to be very similar for both (p,n) and (γ,n) reactions, whereas the higher-energy direct emissions should show a strong forward anisotropy with proton bombardment and a preference for 90° emissions with γ-ray irradiation.

Several attempts were made to fit the low-energy end of the (p,n) and (γ,n) spectra with evaporation-theory predictions, and the best results were obtained with the spectrum derived by LeCouteur[2] and Lang,[3]

$$\sigma(E_n)=\sigma_c E_n^{\lambda} e^{-E_n/T}, \quad (1)$$

where σ_c is the inverse capture cross section of the excited residual nucleus for neutrons of energy E_n, and T the level-density parameter ("nuclear temperature"). The accurate computation of σ_c is not important for analyzing neutron spectra because σ_c varies slowly with emission energy, much unlike the case for analyzing proton and α-particle emission spectra.[4] The exponent λ corrects for some de-excitation of the intermediate nucleus by emission of the first nucleons when more than one nucleon is emitted, and $\lambda\cong5/11$ if the "compound-nucleus" excitation energy E^* has a narrow energy spread[2,3] (the spread in E^* due to energy leakage by the energetic precompound emissions was found to be negligible for the targets heavier than ^{27}Al, where the LeCouteur analysis is most valid, because of the much smaller probability of precompound emissions than of compound emissions). Then, a plot of $\ln[\sigma(E_n)/(\sigma_c E_n^{5/11})]$ versus E_n should provide an unambiguous straight-line fit at low energies where evaporation neutrons predominate, and the higher-energy precompound emissions should show up as an excess above the straight-line boundary. In this respect, the evaporation analysis is valid only when the evaporation (compound) and precompound emissions are well separated in energy.

The "statistical model of intermediate structure" of

* This work supported by National Aeronautics Space Administration under AEC's contract with Union Carbide under Order No. R-104(1) and L-12,186.
† Now at Gulf General Atomic, San Diego, Calif. 92112.
‡ Now at Tennecomp Company, Oak Ridge, Tenn. 37830.
[1] R. R. Harvey, J. T. Caldwell, R. L. Bramblett, and S. C. Fultz, Phys. Rev. 136, B126 (1964).
[2] K. J. LeCouteur, in *Nuclear Reactions*, edited by P. M. Endt and M. Demeur (North-Holland Publishing Co., Amsterdam 1959), Vol. I, Chap. VII.
[3] K. J. LeCouteur and D. W. Lang, Nucl. Phys. 13, 32 (1959).
[4] See, for example, R. Sherr, and F. P. Brady, Phys. Rev. 124, 1928 (1961).

Griffin[5] goes one step further. The (p,n) spectra can be fitted with a linear combination of two curves, one for precompound emissions W_p and one for compound-nucleus emissions $W_c(g)$. The end product of the fitting is a level-density parameter g and the fraction of precompound emissions. This work represents perhaps the first study of the variation of g along the periodic table.

The fraction of precompound emissions is also predicted by the Monte Carlo intranuclear cascade (precompound) code of Bertini[6] combined with a Monte Carlo evaporation (compound) code of the type developed by Dostrovsky, *et al.*[7] This code goes one step beyond that of Griffin's calculations in that no fittings are necessary: The calculated absolute yields versus neutron energy (and emission angle, if desired) are directly compared with the measured results. The Bertini codes were originally written to calculate absolute cross sections versus emission energy for the production of neutrons and charged particles by protons of 50 to several hundred MeV bombarding energy. The present experiments were utilized to help determine the capability of accurately predicting these neutron production cross sections at proton bombarding energies well below 50 MeV, yet well above the threshold for multiple nucleon emission. Thus, 18 MeV represents about the lowest energy for testing the salient features of the Monte Carlo code. Some runs were repeated at 14 MeV, because a preliminary calculation showed a large difference in the spectra below 3 MeV for protons of 14 and 18 MeV on ^{27}Al. Accurate neutron-production calculations are of importance to the shielding of manned space-exploring vehicles from the highly abundant low-energy protons in solar flares and in Van Allen belts, a problem which led to both the motivation and support of the present work.

II. EXPERIMENTAL METHODS

A. (p,n) Reactions

A proton beam from the Oak Ridge National Laboratory isochronous cyclotron was used to irradiate 1- to 2-MeV-thick samples at incident energies of 18.57 and 15.09 MeV, resulting in the average proton energies in the targets, $\bar{E}_p$, shown in Table I. The resultant neutron spectral flux, $\phi(E_n)$, was measured at several angles with respect to the proton beam. By integrating over angle, the neutron-yield cross section $\sigma(E_n)$ was obtained, where

$$\sigma(E_n)=\sigma(p,n)+\sigma(p,pn)+2\sigma(p,2n)+3\sigma(p,3n)\cdots.$$

Because of the inability to separate these several branches of neutron production experimentally, the cross section can be obtained only in laboratory coordinates.

The schematic diagram of Fig. 1 shows a beam of monoenergetic protons passing through a very thin beam-sampling foil and a much thicker target foil (see Table I for thicknesses), and entering a polyethylene-lined secondary Faraday cup. Neutrons leaving the main target at an angle θ can produce counts in the NE-213 organic scintillator shown.

Target thicknesses were measured by carefully weighing a circular area punched out of the center. The proton beam was measured with the secondary CH_2-lined Faraday cup shown in Fig. 1. This was cross calibrated against a more sophisticated main Faraday cup[8] (later removed) with the aid of the thin, retractable polyethylene foil inserted in the beam path. The adjacent ionization chamber with current integrator served as reference for beam intensity during these comparisons. The main current integrator attached to either Faraday cup was periodically calibrated against a standard current source.[9] The secondary CH_2-lined Faraday cup was used during the measurements of neutron spectra because it produced a much lower neutron background than the main Faraday cup. The background was 2% of total for ^{115}In and 30% of total for ^{14}N. It was measured at an incident proton energy E_p rather than at $E_p-\Delta$, where Δ is the energy loss of the protons in a given target (see Table I). To make a minor correction for this, the neutron energy for the background run was reduced by a factor of $(E_{\max}-\Delta)/E_{\max}$ and the area reduced by a factor determined from the slope of published thick-carbon-target neutron yield data[10] extrapolated up to our incident proton energies of 15.09 and 18.57 MeV. The proton energies were measured by Bertrand, Santoro, and Love, using a range-wheel technique.[11]

The neutron scintillation spectrometer has been described elsewhere.[12,13] It utilized a 2-in.-diam by 2-in.-high NE-213 liquid organic scintillator with pulse-shape discrimination to reject γ-ray events. The scintillator was calibrated at a number of neutron energies,[14] a response matrix was derived from this, and neutron energy spectra were subsequently obtained by operating on measured pulse-height distributions with the re-

[5] J. J. Griffin, Phys. Rev. Letters **17**, 478 (1966).
[6] H. W. Bertini, Phys. Rev. **131**, 1801 (1963). For greater detail, see H. W. Bertini, Oak Ridge National Laboratory Reports Nos. ORNL-3383 and ORNL-3433, 1963 (unpublished).
[7] I. Dostrovsky, Z. Fraenkel, and G. Friedlander, Phys. Rev. **116**, 683 (1959); I. Dostrovsky, Z. Fraenkel, and L. Winsberg, *ibid.* **118**, 281 (1960); I. Dostrovsky, Z. Fraenkel, and P. Rabinowitz, *ibid.* **118**, 791 (1960).
[8] R. T. Santoro and R. W. Peelle, Oak Ridge National Laboratory Report No. ORNL-3505, 1964 (unpublished).
[9] R. T. Santoro, F. E. Gillespie, and P. M. Aebersold, Rev. Sci. Instr. **37**, 919 (1966).
[10] R. R. Borchers, J. C. Overley, and R. M. Wood, Nucl. Instr. Methods **30**, 73 (1964).
[11] R. T. Santoro, F. E. Bertrand, T. A. Love, and R. W. Peelle, Oak Ridge National Laboratory Report No. ORNL-TM-1382, 1966 (unpublished).
[12] V. V. Verbinski, F. G. Perey, J. K. Dickens, and W. R. Burrus, Phys. Rev. **170**, 916 (1968).
[13] V. V. Verbinski, W. R. Burrus, R. M. Freestone, and R. E. Textor, International Atomic Energy Agency Symposium on Neutron Monitoring, Vienna, 1966 (unpublished).
[14] V. V. Verbinski, W. R. Burrus, T. A. Love, W. Zobel, N. W. Hill, and R. E. Textor, Nucl. Instr. Methods (to be published).

TABLE I. (p,n) reactions: experimental conditions and results.

Target	$\bar{E}_p$ (MeV)	ΔE (MeV)	f_c Monte Carlo	f_c Griffin theory	g (Levels per MeV)	T^a (MeV)	Thresholds (MeV) (p,n)	(p,pn)	$(p,2n)$	Proton binding energy (MeV)	σ_n above 0.5 MeV (mb)	σ_n total (mb)
^{9}Be	14.4	1.27	···	···			1.9	1.7	20.4	6.6	···	···
^{9}Be	18.0	1.06	0.67	···			1.9	1.7	20.4	6.6	470	545
^{14}N	17.9	1.42	0.23	···			5.9	10.6	···	7.3	84	95
^{27}Al	14.5	1.11	0.07	0.43±0.07	2±1	2.54±0.15	5.6	13.7	···	11.6	321	385
^{27}Al	18.3	0.95	0.30	0.57±0.07	3±1	2.46±0.15	5.6	13.7	···	11.6	209	250
^{56}Fe	18.0	1.09	0.74	0.81±0.05	4±1	1.65±0.15	5.4	11.2	15.4	6.3	859	1010
^{115}In	18.3	0.54	0.86	0.94±0.02	9±1	1.22±0.15	0.3	9.0	7.8	9.1	5840	7190
^{181}Ta	18.0	1.18	0.90	0.89±0.03	13±1	1.04±0.15	1.0	7.6	7.7	7.0	3338	3430
^{208}Pb	14.0	2.09	0.91	0.71±0.03	7±1	1.45±0.15	3.7	7.4	10.6	3.7	···	···
^{208}Pb	17.6	1.82	0.91	0.93±0.04	9±1	1.00	3.7	7.4	10.6	3.7	2822	3370

[a] From plot of $\ln[\phi(E)/\sigma_c E^{5/11}]$ versus E.

sponse matrix. The operation was performed with an unscrambling code written for this purpose.[15,16] A test of the spectrometer consisted of measuring a PoBe neutron spectrum. Agreement in shape with nuclear-emulsion measurements was good,[12,13] and agreement in magnitude with a calibration carried out by the National Bureau of Standards was better than 5%. A californium fission-neutron spectrum is shown in Fig. 2. It is clear that a theoretical fit to our data would be consistent with the illustrated theoretical fits to data of Conde and During,[17] and of Smith and Fields.[18]

Results of the measured spectra for (p,n) reactions were integrated over angle to obtain smooth, featureless spectra for comparison with the theories discussed below. For these measurements, the Faraday-cup and current-integrator calibrations are expected to be accurate to better than 2% and the foil thickness to 2%. Although the neutron spectrometer is accurate to better than 5% in absolute neutron flux under favorable conditions, the high γ-ray count rate due to protons striking the polyethylene beam dump introduced some probable systematic error that could not be determined with precision. Tests were made with an equivalent ^{60}Co γ-ray count rate in the presence of 3-MeV d,d neutrons. These showed negligible spectral distortion above 0.5 MeV, our spectrometer cutoff energy, but since the experimental conditions were only approximately reproduced, an over-all probable error of 20% is suggested for the integrated neutron cross sections.

B. (γ,n) Reactions

Figure 3 shows the experimental arrangement for irradiating the lead isotopes and bismuth with 33-MeV end-point bremsstrahlung obtained with the General Atomic electron linear accelerator. The magnet was used to vary θ, the angle between the electron beam and the neutron-detector flight path. 33-MeV electrons were incident on ~0.5 cm-thick samples of lead (~85% enriched radiogenic ^{206}Pb and ^{208}Pb) and bismuth. The

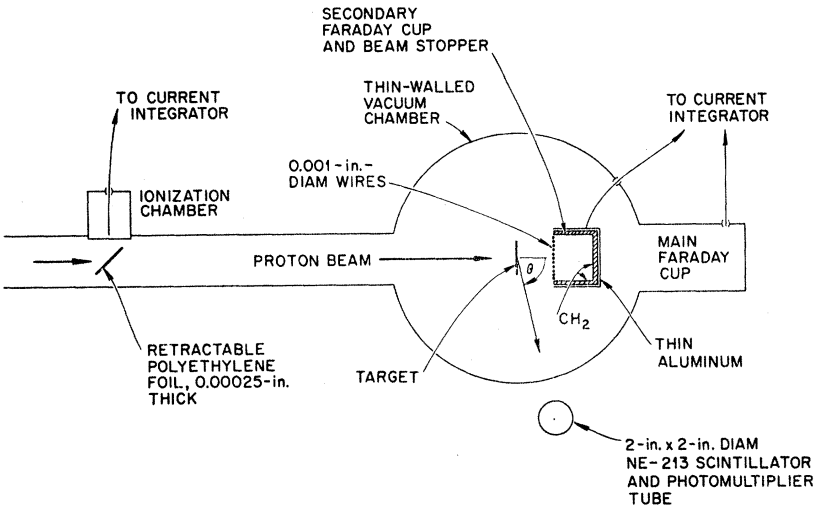

FIG. 1. Experimental geometry for (p,n) spectral yields. The main Faraday cup was removed after calibrating the secondary Faraday cup against it.

[15] W. R. Burrus and V. V. Verbinski, Nucl. Instr. Methods **63**, 237 (1968).
[16] W. R. Burrus and J. D. Drischler, Oak Ridge National Laboratory Report No. ORNL-4154, 1968 (unpublished).
[17] H. Conde and G. During, Arkiv Fysik **29**, 313 (1965).
[18] A. B. Smith and P. R. Fields, Phys. Rev. **108**, 411 (1957).

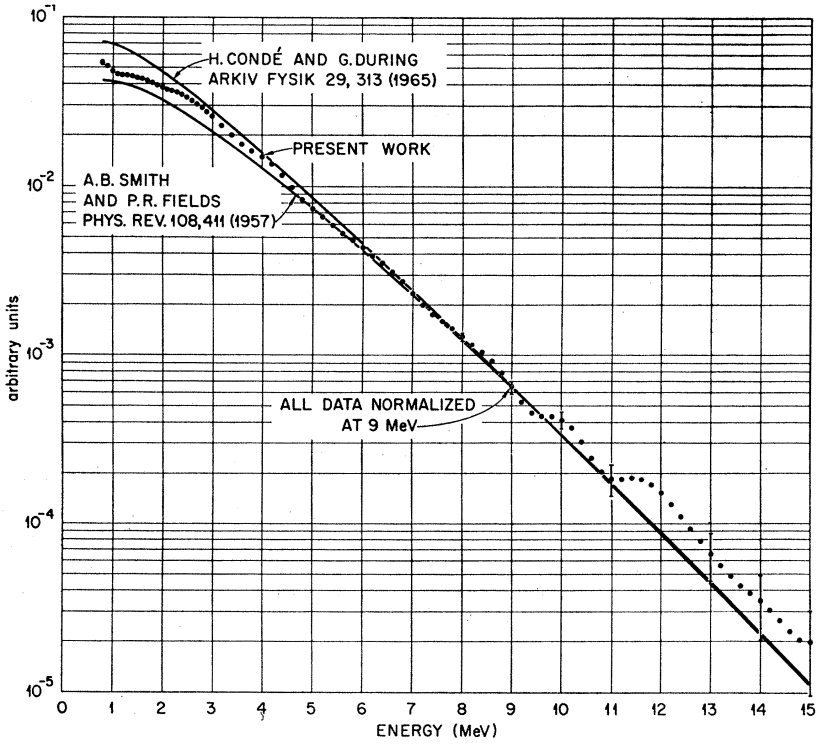

FIG. 2. ^{252}Cf neutron spectrum as measured by unfolding the pulse-height distribution produced in the organic scintillator. The two solid curves are evaporationlike fits to the measurements cited in the two references.

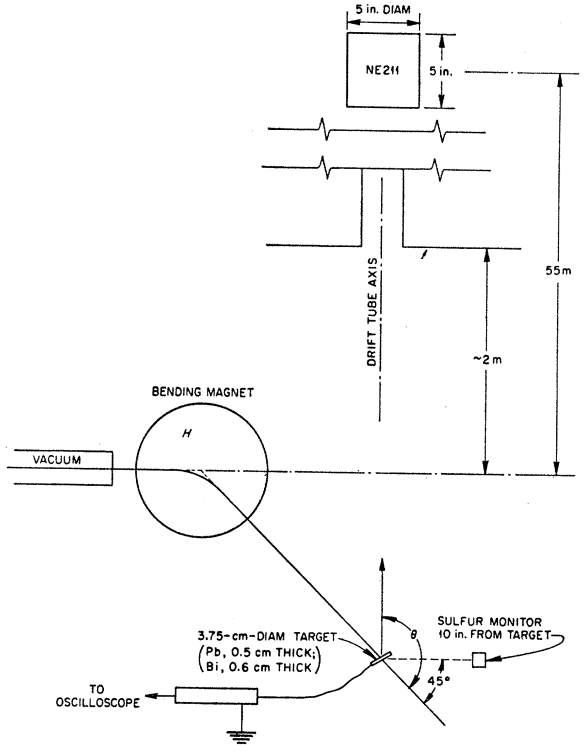

FIG. 3. Experimental geometry showing electron-beam handling, target, neutron drift tube, and detector for time-of-flight neutron spectral measurements on Pb and Bi. For the Al target, a 0.15-cm-thick Bi converter was placed in the magnetic field. (See Ref. 19 for details.)

source of nearly all the neutrons produced in high-Z targets as thick as these is (γ,n) reactions due to bremsstrahlung radiation and not disintegrations produced by electrons.

For the ^{27}Al target, a 0.15-cm-thick bismuth converter placed in the magnetic field of the bending magnet was irradiated by electrons which were then swept out of the way with the remaining magnetic-field region. The aluminum target was placed in the bremsstrahlung beam where it intersected the 55-m neutron drift tube leading to a 5-in.-diam by 5-in.-long NE-213 scintillator. The measuring techniques are discussed in greater detail elsewhere.[19] The use of time-of-flight techniques for measuring neutron spectra from (γ,n) reactions makes these spectra somewhat more reliable than the (p,n) spectra.

III. COMPARISON WITH GRIFFIN'S STATISTICAL MODEL OF INTERMEDIATE STRUCTURE

In this model,[5] the initial state is a 1-particle state in which the excitation energy E^* is determined by the sum of the kinetic and binding energy of the incident proton. This energy is shared by means of a weak 2-body residual interaction which causes transitions between states corresponding to eigenvalues of an independent-particle Hamiltonian. The transitions first give rise to

[19] V. V. Verbinski and J. C. Courtney, Nucl. Phys. **73**, 398 (1965); V. V. Verbinski, J. C. Courtney, and N. Betz, Nucl. Instr. Methods **52**, 181 (1967).

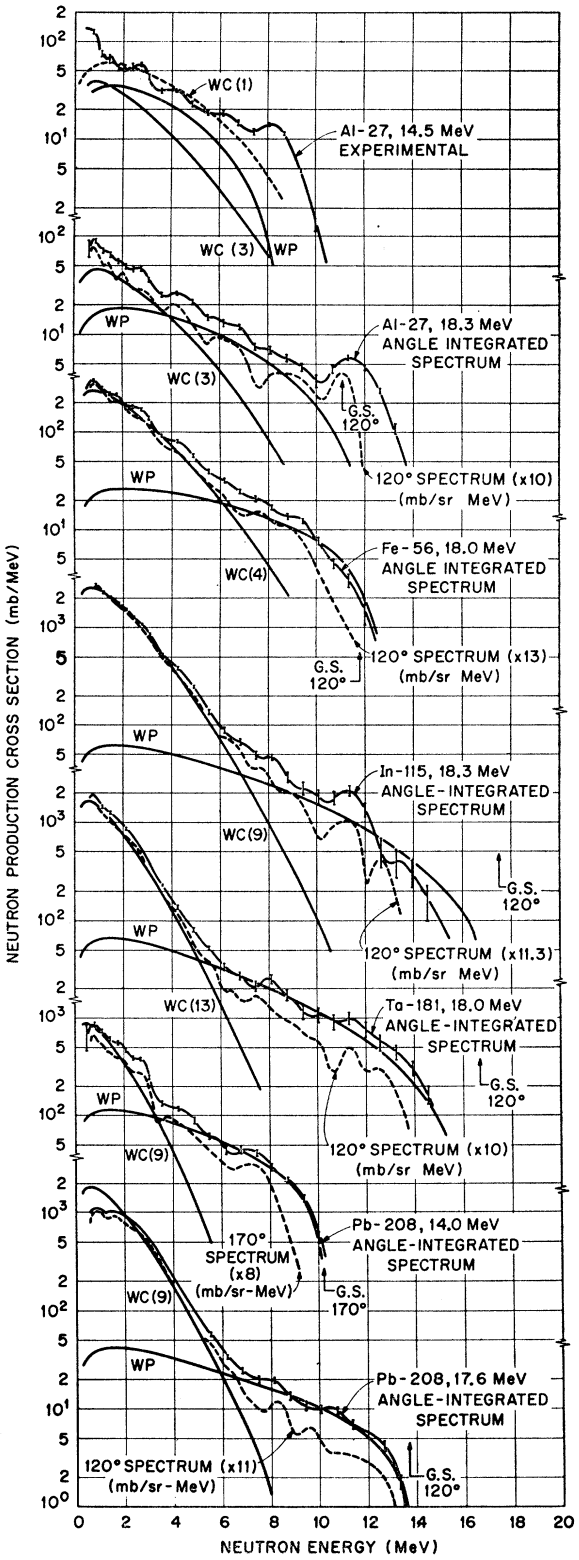

FIG. 4. Angle-integrated experimental neutron production cross sections, $\sigma(E_i)=\sum_j \sigma(E_i,\theta_j)\Delta\Omega$, and cross sections measured at $\theta_j=120°$ and 170°. The $\sigma(E_i)$ are fitted with a precompound component, WP, and a compound component, $WC(g)$, calculated from Griffin's theory (see Ref. 5). The level-density parameter g is obtained from this fitting procedure (see text). G. S. 120° refers to the highest-energy neutron possible, the ground-state transition, at 120° laboratory angle.

3-exciton states (2-particle, 1-hole), then 5, 7, $\cdots$, n. At each transition the probability of neutron emission is calculated, and these early emissions comprise the precompound neutrons whose spectrum is designated as W_p, where

$$W_p \propto \frac{E_p^{1/2}}{E^*}\left(\frac{1+3r^2}{(1-r^2)^3}-1\right) \quad (A \text{ even}), \tag{2a}$$

$$W_p \propto \frac{E_p^{1/2}}{E^*}\left(\frac{3r+r^3}{(1-r^2)^3}\right) \quad (A \text{ odd}), \tag{2b}$$

$r=(U/E^*)$, E_p is the proton bombarding energy, E^* is the excitation energy of the compound nucleus, $U=E^*-(E_n+B)$, the excitation energy of the residual nucleus, and B is the binding energy of the emitted nucleon.

When n approaches its equilibrium value $\bar{n}$, the compound nucleus has been formed. n can readily change by 0 or ± 2 within the constraint of energy conservation, and during these transitions the probability of producing compound-nucleus-decay neutrons $W_c(g)$ is calculated. The approximate expression for $W_c(g)$ used was

$$W_c(g) \propto f(E^*,U)\exp[4(g^2E^*U)^{1/4}], \tag{3a}$$

where

$$f(E^*,U)=E_p^{1/2}(E^*)^{19/8}U^{-11/8}(1+r+r^2) \tag{3b}$$

and g is the density per MeV of single-particle states. Values of g were obtained by fitting the observed angle-integrated neutron spectra with W_p and $W_c(g)$, where g was varied to give the best fit. The fitted neutron spectrum $\alpha W_p+\beta W_c(g)$ also provides $f_c=\beta/(\alpha+\beta)$, the fraction of emerging neutrons resulting from compound nucleus decays. Ignoring shell effects, g should vary as the nuclear volume (as A). The theory should be applied only in regions of A and E^* where $\bar{n}=(gE^*)^{1/2}\gg 1$. This probably excludes the very light targets ^{9}Be and ^{14}N at proton bombarding energies E_p of 14 and 18 MeV, where $\bar{n}\sim 5$, but may nominally include ^{27}Al.

The results of the fitting are shown in Fig. 4. The amplitudes α and β in the expression $\alpha W_p+\beta W_c(g)$ were independently varied to give the best fit to the shape of the experimental spectra. The fitting was repeated for several values of $W_c(g)$, and the value of g was obtained by observing which $W_c(g)$ gave the best final fit. Both the angle-integrated experimental neutron spectrum in laboratory coordinates and a backward-angle spectrum have been fitted with the parameters g and f_c presented in Table I. For ^{27}Al, $W_c(1)$ and $W_c(3)$ are shown to indicate the variation of $W_c(g)$ with g. Note that a lower value of g corresponds to a flatter (harder) spectrum. For the target ^{208}Pb, Fig. 4 shows the results of an attempt to fit the two lead spectra with $\alpha W_p+\beta W_c(9)$, thereby underscoring differences in the two experimental spectra. This gave the best fit for a

proton-bombarding energy E_p of 17.6 MeV, but $W_p(7)$ gave the best fit for $E_p=14$ MeV (not shown in Fig. 4). These data indicate that g increases with E^*, but the experimental accuracy is inadequate to establish this conclusively (see Table I). The fittings show a clear distinction between precompound and compound neutron decays for heavy elements because g is large, making $W_c(g)$ quite steep and negligible in value at the higher neutron energies where W_p still holds up well. From Table I we can see that g varies almost linearly with A, as expected, except for the target ^{208}Pb. The ^{208}Pb spectrum gives $g=9$ at $E_p=18$ MeV, whereas extrapolation by A from Al through Ta gives $g\simeq 15$ for Pb. The dependence of g on A thus shows a definite closed-shell effect. In addition, there is some evidence, admittedly weak, that g increases with increasing E^*. This would be consistent with the picture of a displacement energy ΔE by which the normal level-density values are shifted for closed-shell nuclei.

Figure 4 shows that, in the spectra for neutron emission at 120°, the energy of the ground-state transitions (shown at g.s. 120°) corresponds to the tail end of the neutron spectrum for the ^{27}Al, ^{56}Fe, and ^{208}Pb targets. For ^{115}In and ^{181}Ta, the experimental evidence shows a striking absence of near-ground-state transitions, over and above the effects due to a decrease in E^* after the emission of the first nucleon. This indicates a poor overlap between the wave functions describing the initial states and those describing the low-lying levels of the residual nuclei. The latter are rotational levels that are quite different from the simple 1-particle 1-hole levels produced by the first collision of the captured incident proton and the ejected neutron.

IV. COMPARISON WITH MONTE CARLO CASCADE PLUS EVAPORATION CALCULATIONS

A. Calculations

With the Monte Carlo method and code of Bertini,[6] nucleon-nucleon collisions within a nucleus were followed until each excited nucleon either escaped from the nucleus or lost energy below E_{co}, the cascade cutoff energy. The momentum vectors of the escaped nucleons, the remaining excitation energy, and the identity of the residual nucleus were recorded for use in processing codes which sorted the cascade events into angle and energy bins, and calculated an isotropic evaporation yield. The processing code of Bertini[6] and that of Peelle[20] were used. These were modifications of the EVAP code of Dresner,[21] which was based on a similar code of Dostrovsky *et al.*[7]

The intranuclear cascade code utilized the following assumptions: (i) The nucleon-nucleon collisions could be described by cross sections derived from free-particle cross sections because the reduced deBroglie wavelength of the incident nucleon in the nuclear potential well is generally less than the average internucleon distance; (ii) the separation energy of the most loosely bound nucleon was taken as 7 MeV; (iii) E_{co} was taken to be the same for neutrons and protons; (iv) the neutron and proton densities were approximated by a 3-region nucleus with constant density in each region, the neutron density distribution followed the proton distribution, and the proton density and boundary of each region were adjusted to fit a nonzero Fermi-type charge distribution derived from electron-scattering data; (v) a zero-temperature Fermi momentum distribution was assumed for each region. The use of the 3-region nucleus improved the agreement of the calculation[6] with experimental data above 50-MeV bombarding energy over that obtained with the preceding generation of similar codes.[22] In fact, the code was initially intended for energies above 100 MeV. The present experiments help in determining its validity below 50 MeV and in pointing out computational simplifications which, however adequate at high energy, produce serious errors at low energy.

The EVAP code[21] basically assumes a Weisskopf[23] nuclear level density function, $W(E)=C\exp 2(aE_e)^{1/2}$, where E_e is the effective excitation energy $E-\delta$, δ being the Cameron pairing energy;[24] and the parameter a was taken from LeCouteur's work. Where more than one particle can be emitted, the relative probabilities and spectra are determined stochastically in the program. Unlike the cascade calculations, the evaporation calculations use either measured binding energies, or, where necessary, estimated values.

B. Comparison with Experiment

We carried out the cascade calculations with the cascade cutoff energy E_{co} set at $E_{c/2}$, or 2 MeV, whichever was smaller. $E_{c/2}$ is half the proton Coulomb barrier energy. This value of E_{co} was chosen because of a constraint in the present version of the cascade code in which E_{co} must be the same for protons and neutrons, and because higher values produce a dip in the cascade-plus-evaporation neutron spectrum just below E_{co}. This low value of E_{co} made very little difference in the evaporation yield above 6 MeV for the test case, ^{181}Ta, for which E_{co} was taken first as $E_{c/2}$, then as 2 MeV.

In comparisons of calculation and experiment presented in Fig. 5, perhaps the most obvious defect is that of a 7-MeV binding energy for the most loosely bound nucleon. All of the calculational spectra except that for ^{9}Be extend out too far in energy. Use of the correct binding energy would be expected to rectify the situa-

[20] R. W. Peelle and P. M. Aebersold, Oak Ridge National Laboratory Report No. ORNL-TM-1538, 1966 (unpublished).
[21] Lawrence Dresner, Oak Ridge National Laboratory Report No. ORNL-CF-61-12-30, 1961 (unpublished).
[22] N. Metropolis, R. Bivins, M. Storm, Anthony Turkevich, J. M. Miller, and G. Friedlander, Phys. Rev. **110**, 185 (1958); **110**, 204 (1958).
[23] V. F. Weisskopf, Phys. Rev. **52**, 295 (1937).
[24] A. G. W. Cameron, Can. J. Phys. **36**, 1040 (1958).

tion for all cases except ^{115}In and ^{181}Ta, where the measurements show a scarcity of near-ground-state transitions that are not taken into account in the structureless cascade code. This was discussed in Sec. III above. Except for ^{115}In and ^{181}Ta, correction for the wrong binding energy could apparently be accomplished by simply reducing the energy scale for the direct reactions by the appropriate amount. The height of the cross-section versus neutron-energy plot apparently changes very little in the plateau region with a change of binding energy, judging from the small change in plateau height with change of bombarding energy from 15 to 18 MeV for ^{27}Al and ^{208}Pb. Thus, the calculation appears to estimate the absolute cross section with fairly good accuracy.

The calculated evaporation yields are somewhat low, as can be seen in the case of ^{27}Al for $E_p=15$ MeV and ^{115}In at $E_p=18$ MeV. In the former case, the cascade cutoff is at nearly 1.5 MeV. Below this, a very low evaporation yield can be seen. In Table I, this is given as only 7% of total. For $E_p=18$ MeV, the calculation gives 30%, which is in somewhat better agreement with the value of 57% obtained from the Griffin-theory fitting. For targets heavier than ^{27}Al, both theories are much more valid, and agreement is much better (see Table I).

Two other items of interest in Fig. 5 are the very good agreement of the calculation with the ^{9}Be case at $E_p=17$ MeV, and the very poor agreement for ^{14}N. The good agreement for ^{9}Be partially results from the structure being washed out by integration over angle, by target thickness (see ΔE in Table I), and by the confluence of the (p,n) and (p,pn) thresholds. Note that the 7-MeV calculational (p,pn) threshold causes the calculated curve to cross the experimental curve at 7 MeV below E_n(max). For the ^{14}N$(p,n)^{14}$O reaction, the structureless cascade calculation does not take into account the large energy gap between ground and first excited states of the residual nucleus ^{14}O. In fact, the apparent peak at 9 MeV for this angle-integrated spectrum is simply due to the strong ground-state transition at 120° and 170° for ^{14}N, and to the absence of any other measurements above 80°. (See Sec. IX.)

No systematic comparisons of measurements and Monte Carlo calculations were made for angular distributions, but a comparison for the ^{27}Al-target results at 1–3, 3–6, and above 6 MeV, showed a considerably greater forward anisotropy predicted by the calculations than obtained from the measurements given in Sec. VIII.

V. COMPARISON OF THE (p,n) SPECTRA WITH LeCOUTEUR'S EVAPORATION ANALYSIS

In Fig. 6, the logarithmic plots of $\sigma(E_n)/(\sigma_c E_n^{5/11})$ are shown, with the inverse capture cross section σ_c ob-

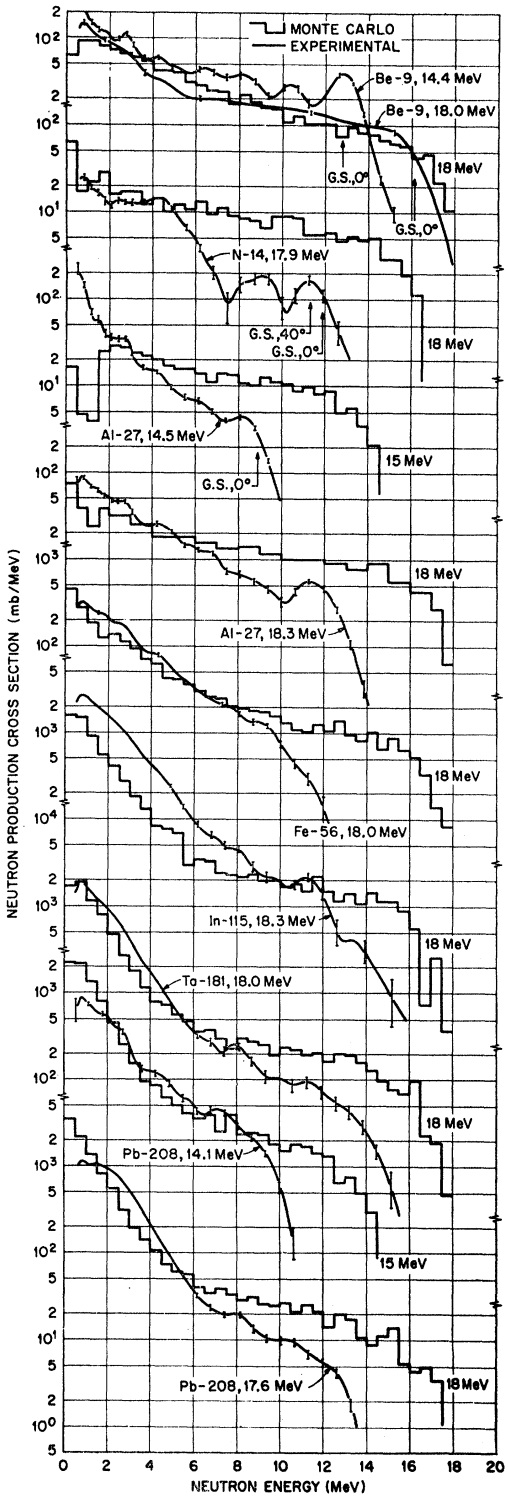

FIG. 5. Angle-integrated experimental spectra compared with Monte Carlo cascade-plus-evaporation calculations. The average proton energy in the target material is shown. G. S. 0° is the ground-state neutron for (p,n) reactions, the highest-energy neutron possible. For nuclei heavier than ^{27}Al, G. S. 0° is not shown, but it is nearly equal to G. S. 120° and 170° shown in Fig. 4.

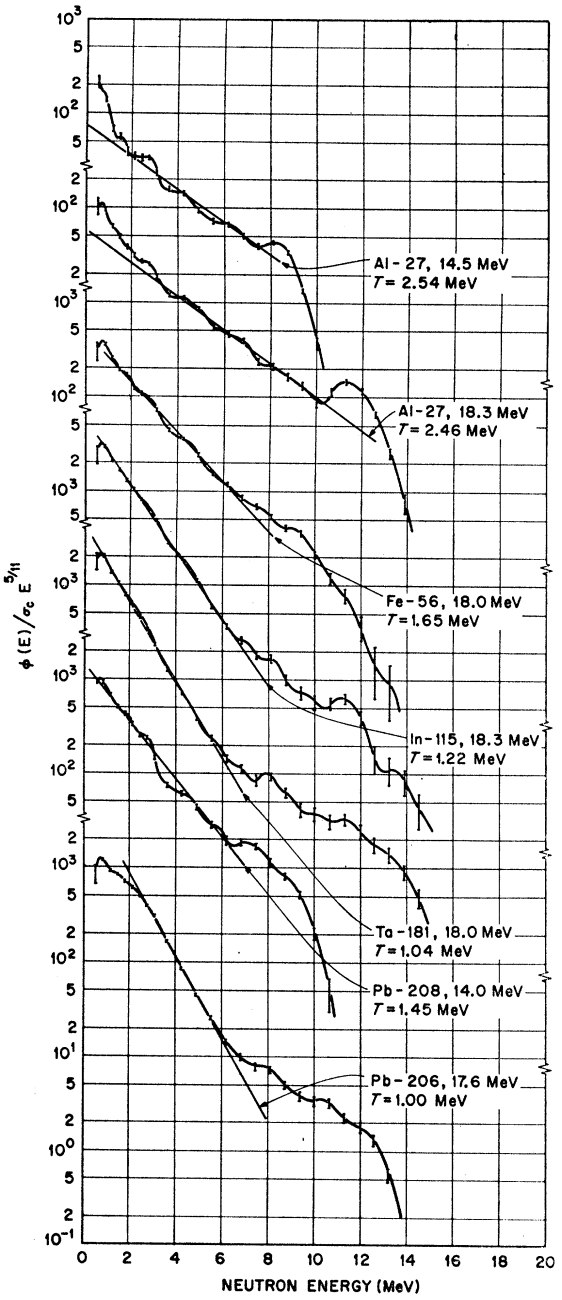

FIG. 6. Evaporation-analysis plots of neutron spectra from (p,n) reactions. The neutron spectra are divided by the product of σ_c and $E_n^{5/11}$, according to the analysis of LeCouteur (Ref. 2). Above 6 MeV, a "direct-reaction" excess is seen above the straight-line fit. The slope of the straight line is steep for heavy nuclei, which results in a clear separation of compound and direct neutron emissions. For ^{27}Al, the slope is probably the result of a significant admixture of direct-emission neutrons.

tained from the continuum-theory calculations.[25] According to the analysis of LeCouteur,[2,3] the exponent λ [see Eq. (1)] of the divisor E_n should equal 5/11 if E^* is both narrow in energy spread and well above the (p,pn) and $(p,2n)$ thresholds. For all measurements with targets heavier than ^{27}Al, E^* is above the (p,pn) and $(p,2n)$ thresholds. In addition, Secs. III and IV indicate that the evaporation yield is over five times the yield of precompound neutron emissions. Thus, it seems safe to conclude that the spread in E^* of the compound nucleus, caused by precompound "energy leakage," is too small to invalidate the LeCouteur evaporation analysis.

The plots in Fig. 6 can each be fitted reasonably well with a straight line whose slope

$$1/T=(d/du)[\ln w(A,U)],$$

where w is the level density of the residual nucleus at excitation energy U. Even the borderline case of ^{27}Al yields a fair straight-line fit.

The "nuclear temperature" T in Fig. 6 is about the same for ^{27}Al at $E_p=14.5$ and 18.3 MeV. It shows a monotonic decrease with increasing A, from ^{27}Al to ^{181}Ta, which is consistent with an increase in level density $w(A,U)$ with A for roughly the same values of U. For ^{208}Pb, the value of T for $E_p=17.6$ MeV is about the same as for Ta^{181}, but for $E_p=14$ MeV T is considerably higher. The average value of T at $E_p=14$ and 18 MeV for ^{208}Pb breaks the trend of T decreasing with A, and reflects a lower nuclear level density because of shell structure. The curve for ^{208}Pb at $E_p=17.6$ MeV is unlike all the other spectra because it has either a bump above 2 MeV or a lack of neutrons below 3 MeV. This is not likely to be an accident of measurement, because nearly the same shape was observed at all angles. Until this shape is understood, it is not clear that a comparison of the slope between 3 and 6 MeV to the slopes of the other 6 curves will be meaningful.

Note for all cases the excess of high-energy neutrons above the extrapolated straight line. For the target nuclei heavier than ^{27}Al, the Monte Carlo results given in Table I show about 75% or more of evaporation neutrons. The straight-line fits at lower energies should be representative of the true evaporation yield, and the excess of high-energy neutrons should be due to direct reactions.

The values of T given in Table I and Fig. 6 for ^{27}Al and ^{56}Fe are considerably lower than those reported by Gugelot.[26] Most of the disagreement is due to the difference in analysis of the data: The spectra presented here were divided by $\sigma_c E_n^{5/11}$ while those of Gugelot were divided by E_n. The work of Gugelot predates the statistical-nucleus derivations of LeCouteur,[2] which give $\lambda=5/11$ in Eq. (1), to account for multiple nucleon emission.

VI. COMPARISON OF THE (γ,n) SPECTRA WITH LeCOUTEUR'S EVAPORATIONAL ANALYSIS

In Fig. 7, four pairs of neutron spectra are shown for ^{27}Al, ^{206}Pb, ^{208}Pb, and ^{209}Bi in the form of

[25] J. M. Blatt and V. F. Weisskopf, *Theoretical Nuclear Physics* (John Wiley & Sons, Inc., New York, 1952).

[26] P. C. Gugelot, Phys. Rev. 81, 51 (1951).

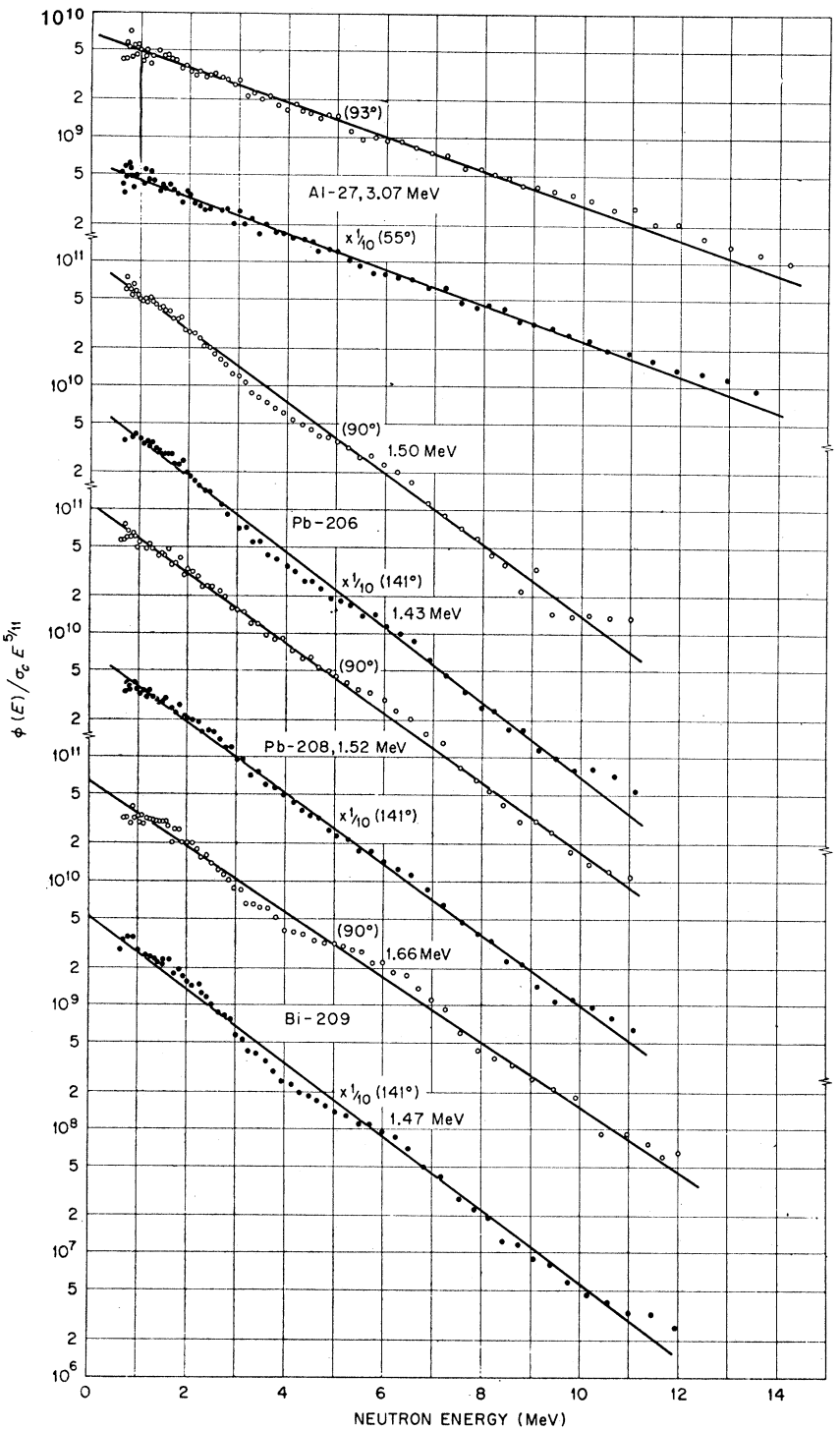

FIG. 7. Evaporation-analysis plots of neutron spectra from (γ,n) reactions. The logarithmic plots of $\phi\ (E)/(\sigma_c E^{5/11})$ show moderately good straight-line fits. Values of T, the magnitude of the reciprocal slope, are shown. In some cases, T is slightly higher at 90° than at 141°, indicating that a weak component of direct emissions is present. These are preferentially emitted at 90°, the direction of the electromagnetic field.

$\ln[\sigma(E)/\sigma_c E^{5/11}]$ versus E plots. All the plots yield reasonably good straight-line fits, indicating that the analysis of LeCouteur[2] is applicable. The values of T obtained from the slope of the line are also given, where the slope is $-1/T$. Note that in some cases the fitted T is higher for the 90° data than for the 141° data. This tendency probably arises from a small admixture of direct-neutron emissions at 90°, the direction of the γ-ray electromagnetic field.

For ^{27}Al, the excitation energy E^* is about 20 ± 2 MeV, because of the giant dipole resonance (γ,n) peak. The "nuclear temperature" T is 3.07 MeV according to the plot shown in Fig. 7 (also see Table II). In the case of the ^{27}Al(p,n) reaction presented in the preceding

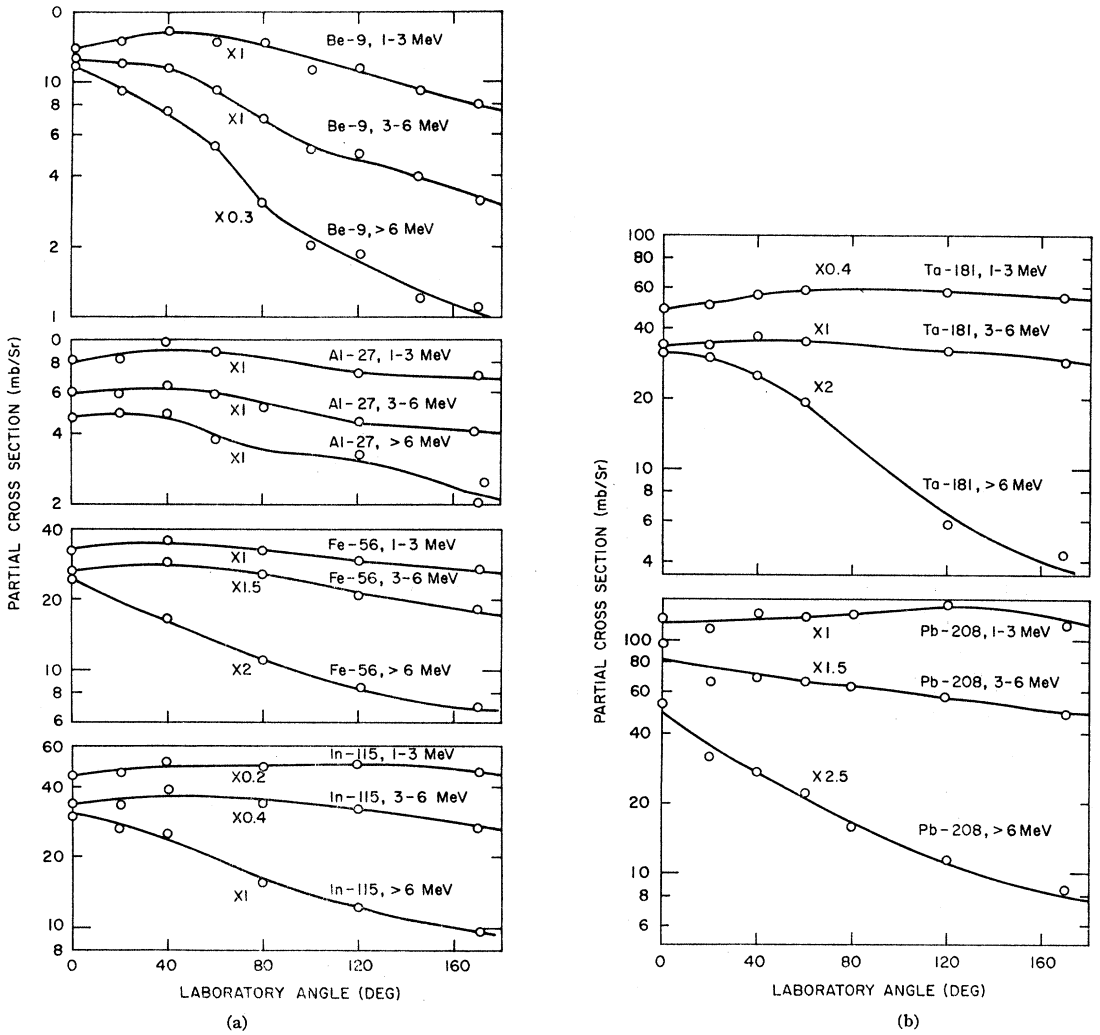

FIG. 8. Experimental angular distributions for neutrons in the energy ranges of 1–3, 3–6, and greater than 6 MeV for proton bombarding energies of about 18 MeV.

section, E^* was 27.5 and 31.3 MeV for $E_p=14.5$ and 18.3 MeV, respectively, and $T\simeq 2.5$ MeV for both bombarding energies. This significantly lower value of T for a considerably larger value of E^* may simply mean that the precompound or direct-reaction neutrons are present in large proportions even at low neutron energies. Evidence of this can be found in Table I, where both the Griffin-theory fitting and the Monte Carlo results indicate that ^{27}Al (p,n) reactions go by way of direct reactions for the most part. If so, the evaporation analysis of the ^{27}Al (p,n) data is meaningless. The direct (p,n) reactions are expected to be different from either direct or compound-nucleus (γ,n) reactions, as was observed.

TABLE II. (γ,n) reactions induced by 33-MeV end-point thin-target bremsstrahlung.

Target	$\bar{E}_\gamma$ giant resonance peak (MeV)	θ	T[a] (MeV)	Thresholds (γ,n)	(γ,pn)	$(\gamma,2n)$
^{27}Al	~22	55°	3.07±0.1	13.1	19.4	24.4
		93°	3.07±0.1			
^{206}Pb	~13	90°	1.50±0.1	8.0	14.8	14.8
		141°	1.43±0.1			
^{208}Pb	~13	90°	1.52±0.1	7.4	14.8	14.1
		141°	1.52±0.1			
^{209}Bi	~13	90°	1.66±0.1	7.4	11.1	14.3
		141°	1.47±0.1			

[a] From plot of $\ln[\phi(E)/\sigma_c E^{5/11}]$ versus E.

For the reaction ^{209}Bi(γ,n) ^{208}Bi, $\bar{E}^*\sim 14$ MeV, or slightly above the center of the giant resonance (γ,n) peak of 13.5 MeV.[4] For the ^{208}Pb (p,n) ^{208}Bi reaction, the same residual nucleus is formed, and $E^*=17.7$ MeV for a bombarding energy $E_p=14$ MeV. The corresponding values of T given in Tables I and II are the same within experimental error, indicating that the low-energy neutrons are mostly emitted from the compound nucleus for both the (γ,n) and the (p,n) reactions. This is consistent with the Monte Carlo results, shown in

Table I, which predict a 90% evaporation yield of (p,n) neutrons.

VII. TOTAL NEUTRON-YIELD CROSS SECTIONS FOR (p,n) REACTIONS

The neutron-yield cross sections above the spectrometer cutoff energy of 0.5 MeV are given in Table I, along with the estimated total cross section. This estimate simply assumes that the neutron production between 0 and 0.5 MeV is equal to that between 0.5 and 1 MeV.

Note how much larger the ^{9}Be (p,n) cross section is than that for ^{14}N, presumably because the neutron outside the closed $1p_{1/2}$ subshell has a very small binding energy and therefore a very large radius. From ^{14}N to ^{115}In, the cross section rises monotonically. It decreases monotonically from ^{115}In to the doubly magic ^{208}Pb, possibly a binding-energy effect. Note that the (p,n) thresholds given in Table I increase monotonically from a low of 0.3 MeV for ^{115}In to a value of 3.7 MeV for ^{208}Pb.

VIII. ANGULAR DISTRIBUTIONS FOR (p,n) REACTIONS

In Figs. 8(a) and 8(b), the experimental angular distributions are shown for energy intervals of 1–3, 3–6, and above 6 MeV. The region above 6 MeV displays the most forward-peaked angular distributions of the three. In this same energy region, the evaporation-analyzed energy spectra of Fig. 6 all show an excess above the straight-line fit. These are identified as precompound neutrons which are best separated from compound-nucleus decays for the targets ^{181}Ta and ^{208}Pb at $E_p=18$ MeV. In addition, the angular distributions for these two cases are the most forward peaked, which reinforces the hypothesis that the neutrons that contribute to the excess above the straight-line fit in Fig. 6 are precompound neutrons.

The angular distribution is the flattest for the case of ^{27}Al at 18 MeV, which fact by itself would suggest that a larger fraction of evaporation neutrons is present than for any other target. This is not consistent with any of the tested models and helps to confirm that these models are applicable only to heavy nuclei. For light nuclei, the identification of reaction mechanisms as either the direct or the compound-nucleus type must proceed along other lines such as studying angular distributions for isolated levels.[12]

IX. NEUTRON SPECTRA AND NEUTRON YIELDS AS A FUNCTION OF ANGLE

In Fig. 9, the cross section versus neutron energy E_n is shown in the laboratory system for nine angles between 0° and 170° for ^{9}Be(p,n) reactions at $E_p=18$ MeV. The c.m. angular distribution of the ground-state transition (shown by arrow) can be deduced from these data. It is characterized by a high forward peaking as well as some background peaking. A distorted-wave optical-model calculation, possibly with the inclusion of the heavy-particle stripping of Owen and Madansky,[27] might reproduce the observed angular distribution. But until such an analysis is successfully carried out, it

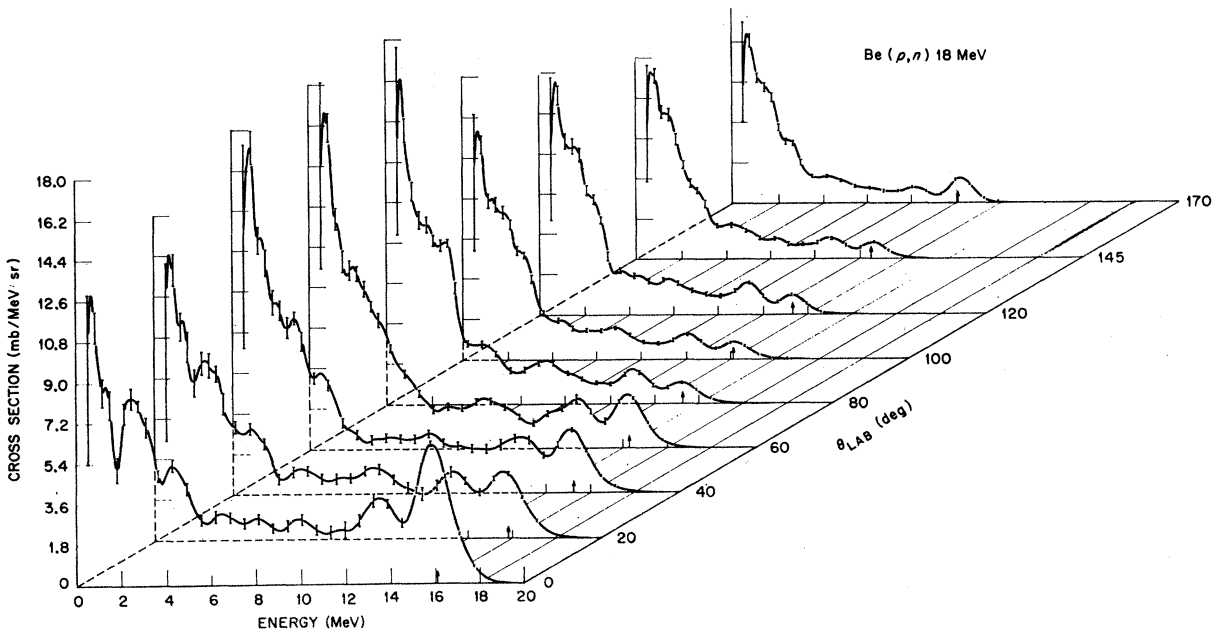

FIG. 9. Neutron spectra and production cross sections for ^{9}Be(p,n) reactions at $E_p=18$ MeV. The yield at about $\frac{1}{2}$–$1\frac{1}{2}$ MeV is slightly depressed at forward angles due, in part, to the 4-mm-thick polyethylene beam stopper in the secondary Faraday cup.

[27] G. E. Owen and L. Madansky, Phys. Rev. **105**, 1766 (1957).

would be unreasonable to exclude a compound-nucleus process involving overlapping of levels, even with the rather large level spacing in this particular case.

The low-energy neutrons are suggestive of an evaporation-type component. The spectral shape could also be explained by a many-body breakup of the ^{10}B intermediate nucleus, similar to the type of multiple-particle breakup observed in the ^{9}Be(α,n) reactions at α-bombarding energies as low as 6 MeV.[12] However, the (α,n) neutrons were highly forward-peaked, whereas the low-energy (p,n) neutrons are much more isotropic and therefore more reasonably attributed to evaporation-type events.

The ground-state transition for the ^{14}N$(p,n)^{14}$O reaction is well isolated as can be seen in Fig. 10. The first excited level and its neighbors near 6 MeV in ^{14}O give rise to the huge peak below the ground-state-transition peak. Except for a variation with angle that is a result of the use of the laboratory frame of reference, the cross section is reasonably constant with angle. The ground-state transitions display a fore-aft peaking, while transitions to states near 6 MeV in ^{14}O are nearly symmetric, assuming that only ^{14}N$(p,n)^{14}$O reactions contribute. Some neutrons that appear above and below the ground-state peak are due to inaccurate subtraction of background neutrons produced by the ^{13}C in the beam stopper and the melamine target. This background was fractionally much lower in all the other targets.

For the ^{27}Al(p,n) reactions at 18 MeV shown in Fig. 11, again there is little angular variation of the cross section versus E_n. The ground-state transition displays a noticeable peaking at about 40°.

In Fig. 12, the ^{56}Fe(p,n) reactions show a strong transition to an isobaric analog state a few MeV above the ground state. These have been observed as a function of angle with good energy-resolution measurements by J. D. Anderson *et al.*,[28] and they were found to be very forward peaked. If we ignore the 0° results below 2 MeV, as well as the analog peak, we can see that the cross section is remarkably constant with angle, and that ground-state transitions are vanishingly small.

For ^{115}In(p,n) reactions the data in Fig. 13 show a vanishingly small cross section for ground-state transitions, as well as for transitions many MeV above the ground-state level in the residual nucleus. Above 6 MeV, the cross section noticeably decreases with angle, while below 6 MeV there is much less change with angle. The same remarks apply for the ^{181}Ta(p,n) reactions shown in Fig. 14, as well as for the ^{208}Pb(p,n) reactions shown in Fig. 15, except that near-ground-state transitions are much more abundant for ^{208}Pb.

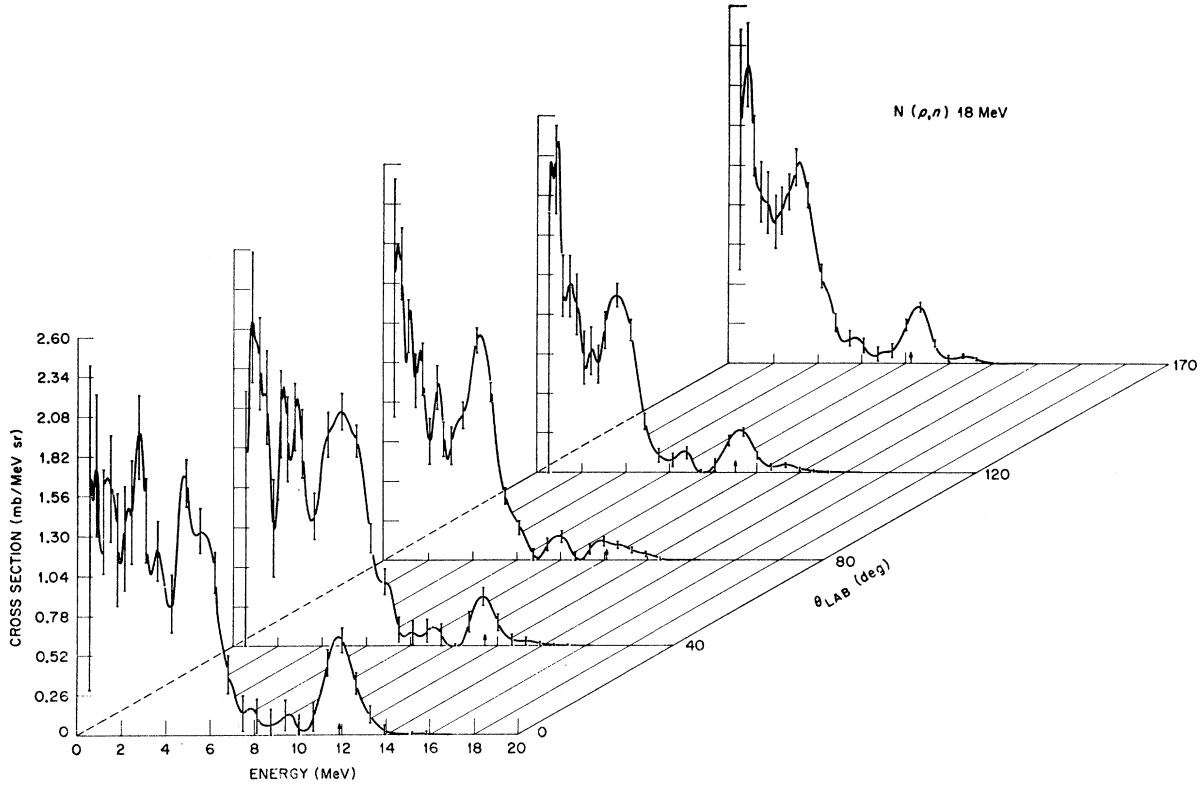

FIG. 10. Neutron yields versus energy and angle for ^{14}N(p,n) reactions at $E_p=18$ MeV.

[28] J. D. Anderson, C. Wong, J. W. McClure, and B. D. Walker, Phys. Rev. **136**, B118 (1964).

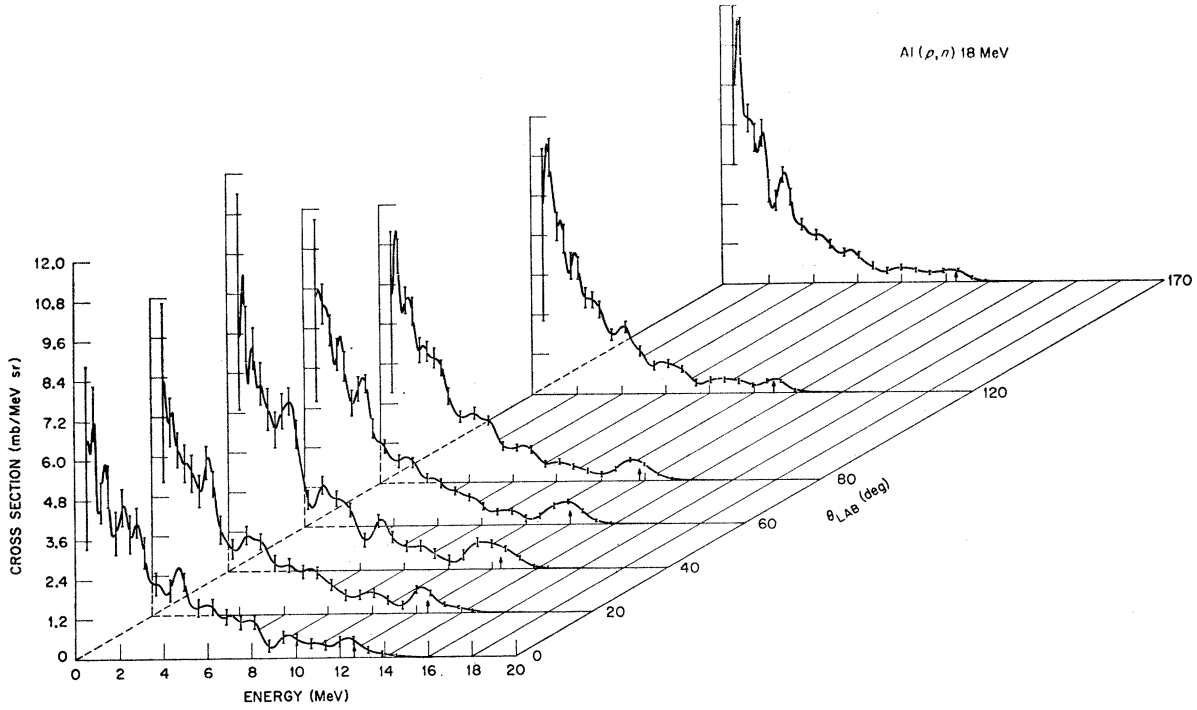

FIG. 11. Neutron yields versus energy and angle for $^{27}Al(p,n)$ reactions at $E_p=18$ MeV.

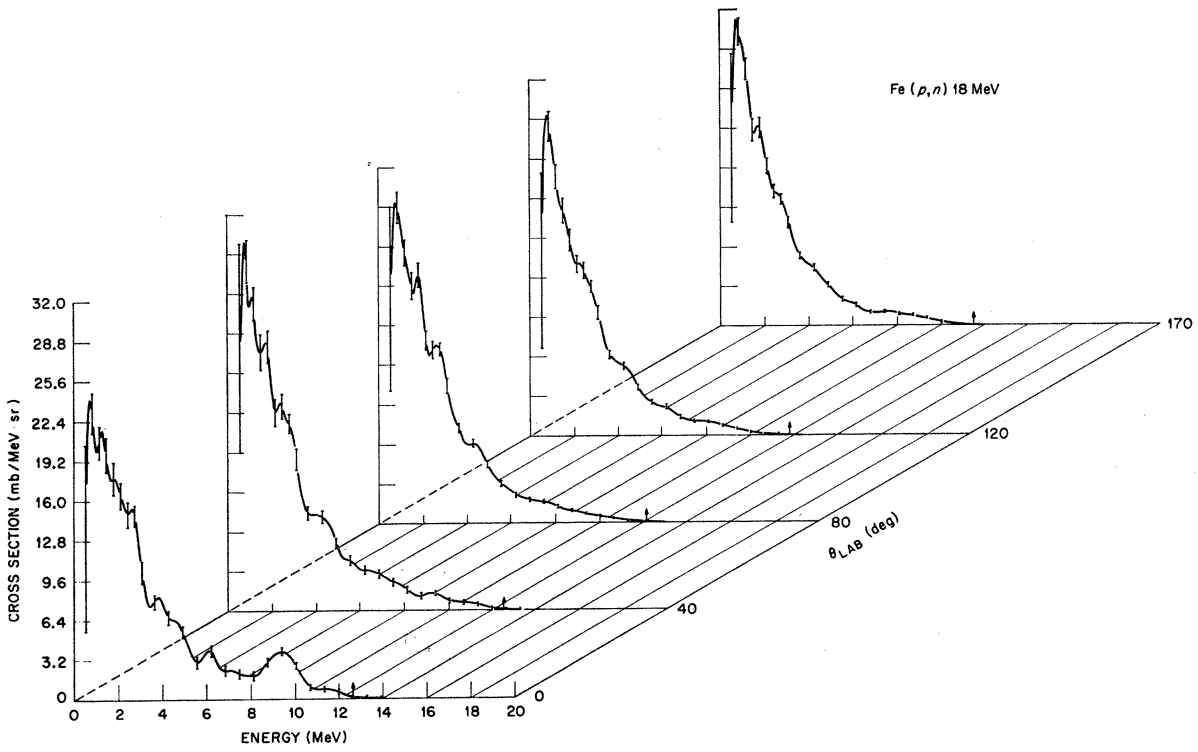

FIG. 12. Neutron yields versus energy and angle for $^{56}Fe(p,n)$ reactions at $E_p=18$ MeV.

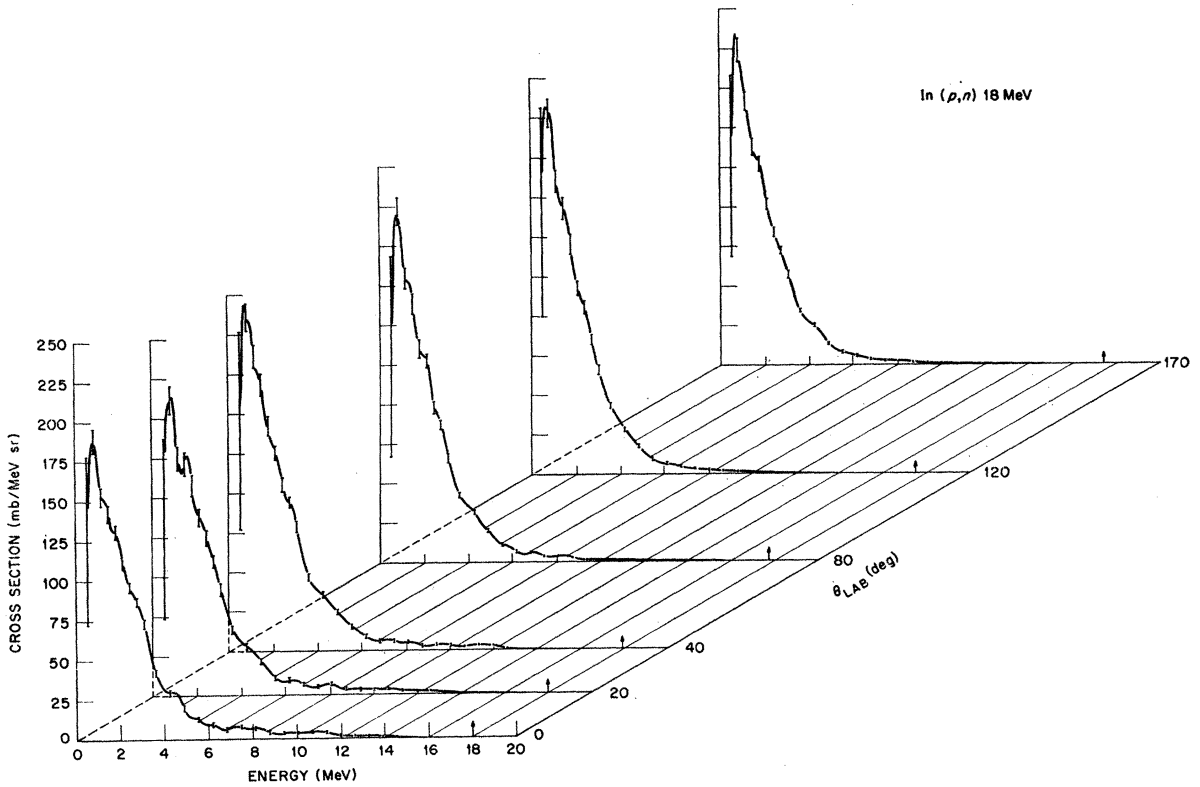

FIG. 13. Neutron yields versus energy and angle for ^{115}In(p,n) reactions at $E_p=18$ MeV.

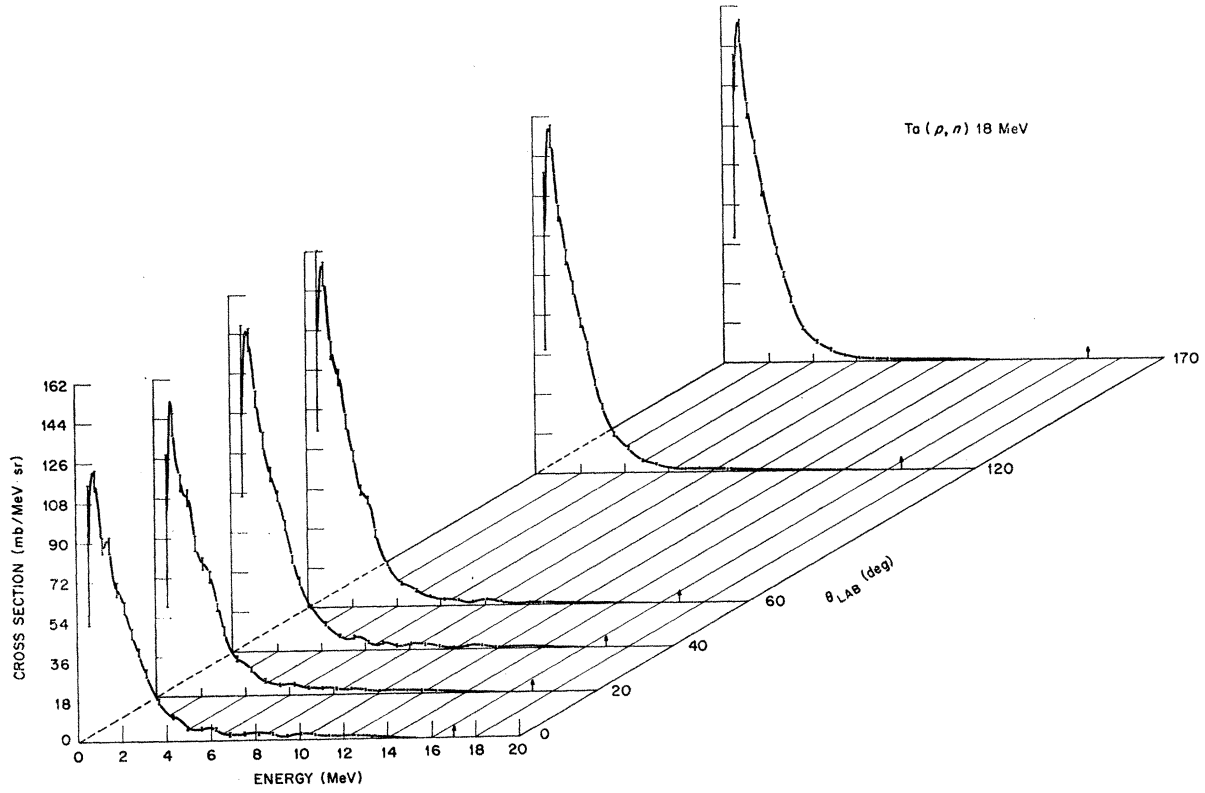

FIG. 14. Neutron yields versus energy and angle for ^{181}Ta(p,n) reactions at $E_p=18$ MeV.

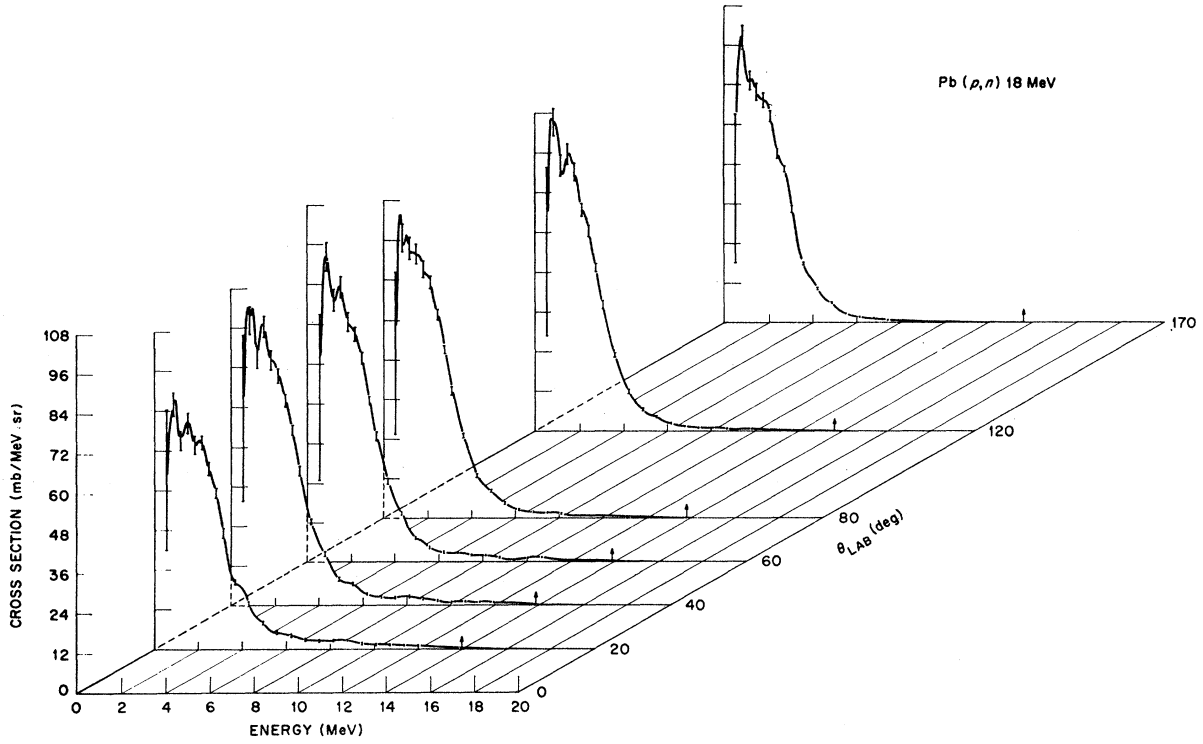

FIG. 15. Neutron yields versus energy and angle for ^{208}Pb(p,n) reactions at $E_p=18$ MeV.

X. SUMMARY AND CONCLUSIONS

The differential (p,xn) cross sections with respect to neutron energy and laboratory angle displayed a forward peaking at neutron energies above 6 MeV, over and above that due to c.m. motion (see Fig. 8). This is consistent with a significant contribution of the direct or precompound-type reaction at high neutron-emission energy. The (γ,xn) spectra and yields, although measured with much better energy resolution, were smoother and were nearly constant with angle, showing little evidence of direct effects at any neutron energy.

The (p,xn) spectra displayed considerable structure which was smoothed by integration over angle, making them suitable for comparison with three types of calculations that were structureless with respect to A dependence, shell effects, etc. Fitting of the (p,n) spectra with linear combinations of Griffin's precompound spectrum W_p, and compound-nucleus-emission spectra $W_c(g)$, produced g the density of independent particle states, and f_c the compound-nucleus fraction. This fitting yielded values of g that increased linearly with A from $g\simeq 2$/MeV for ^{27}Al to $g\simeq 13$ for ^{181}Ta, but decreased to $g\simeq 8$ for ^{208}Pb. The presence of shell effects is clearly established. The data indicate, but do not clearly establish, a decrease in shell effects with excitation energy E^* of the intermediate nucleus, since g appears to increase with E^* for ^{208}Pb (see Table I). The Griffin-theory fitting was most valid at high A, where the precompound and compound spectra are well separated on the energy scale, but was questionable for ^{27}Al where both types of spectra were similar in shape.

Monte Carlo intranuclear-cascade-plus-evaporation calculations predicted values of the compound-nucleus fraction f_c in fair agreement with Griffin-fitting results, where $f_c=0.75$ to 0.90 from ^{56}Fe to ^{208}Pb, but differed significantly for ^{27}Al. The Monte Carlo results agreed rather well with the measurements, but a few flaws in the calculations were clearly evident. Most of them seem correctable. The relative scarcity of near-ground-state transitions in the measured cross sections for ^{115}In and ^{181}Ta indicates a low transition probability from an initial particle-hole configuration to low-lying collective states. The calculations do not, of course, take this into account.

Comparison of the angle-integrated (p,n) spectra with LeCouteur's evaporation-type spectra for multiple-nucleon emission gave good fits at low neutron energies, and yielded the same "effective nuclear temperature" T for both (p,n) and (γ,n) reactions proceeding by way of the intermediate nucleus ^{209}Bi and for excitation energies E^* within a few MeV. But for the target ^{27}Al, the slope parameter T was considerably lower for (p,n) reactions, even though E^* was considerably higher. At such a low value of A, the direct and evaporation components are not clearly separable by energy de-

pendence, and the slope-parameter T therefore becomes meaningless.

It is clear that the three types of calculations or analyses used here to extract information about the nature of the reaction mechanisms are at their best when applied to heavy nuclei.

ACKNOWLEDGMENTS

Thanks are due to F. C. Maienschein for continued encouragement and interest; to R. W. Peelle for many helpful discussions and for the use of his BERDBIND analysis and evaporation code; to H. W. Bertini and M. P. Guthrie for supplying and modifying the LECC10 intranuclear cascade calculations and evaporation calculations that utilized the LECC10 output-tape histories; to R. G. Alsmiller, Jr., for discussions and interpretations of the Monte Carlo calculations; to M. Young for help with data-taking and development of the FERDOR unfolding code; to T. A. Love, R. T. Santoro, F. E. Bertrand, and G. T. Chapman for help with cyclotron beam alignment and energy calibration; to J. C. Courtney for help with the (γ,n) experiments; and to J. R. Beyster of General Atomic for supplying the bending magnets needed for the (γ,n) experiments.

PHYSICAL REVIEW VOLUME 177, NUMBER 4 20 JANUARY 1969

Studies on the Decay of Ge^{67}†

H. BAKHRU AND I. M. LADENBAUER-BELLIS
Yale University, New Haven, Connecticut 06520

(Received 26 June 1968)

The excited levels of Ga^{67} have been investigated from the decay of Ge^{67} with Ge(Li), Si(Li), and standard scintillation counters. γ rays of the following energies were observed: 166.5, 360, 558, 576, 661, 710, 720, 728, 828, 900, 915, 981, 1082, 1116, 1283, 1450, 1677, 1509, 1644, 1810, 1837, 2004, 2100, 2170, 2210, 2510, 2559, 2726, 2958, 2991, 3065, and 3157 keV. The half-life of Ge^{67} was measured to be 19±0.3 min. With the help of γ-γ coincidence studies, a consistent level scheme of Ga^{67} at 166.5, 333, 828, 1082, 1450, 1810, 2170, 2726, 3157, and 3398 keV has been obtained. Three major positron groups with end-point energies of 3.18 MeV (65%), 2.5 MeV (~25%), and 1.54 MeV (<10%) have been assigned to the decay of Ge^{67}. Each group probably consists of more than one component. The results including spin and parity assignments of some of the excited levels of Ga^{67} are discussed. The half-life of the 166-keV level is measured by delayed coincidence to be less than $(0.22\pm0.05)\times10^{-9}$ sec.

1. INTRODUCTION

THE decay of the 19-min isotope of Ge^{67} has been previously studied by two groups of investigators.[1,2] Aten[1] in 1956 first reported a 2.9-MeV positron branch attached to this isotope. These authors also reported only one strong γ ray with an energy of 170±10 keV. The level scheme as shown in *Nuclear Data Sheets*[3] was presented by Ricci and Van Lieshont.[2] These authors reported a γ ray of 170±10 keV in coincidence with another 170-keV γ line. Upon examining the information in Ref. 3, however, it is evident that many of the γ rays have not been fitted into a decay scheme. Even the energy of the second excited state in Ga^{67} is not precisely known.

With the availability of high-resolution solid-state counters, the present work proposes to reexamine the decay of Ge^{67} to establish a level scheme of Ga^{67} with good energy determination.

2. SOURCE PREPARATION

Ge^{67} was produced from Zn^{64} by an (α, n) reaction, using ~19-MeV α particles from the heavy-ion accelerator. The targets used were thin foils of natural Zn. The energy of the α particles and the time of the bombardment were kept low, to avoid any $(\alpha, 2n)$ products. The bombardment time chosen was about 15 min. After cooling the Zn target for 2 min, the following chemical separation was performed. The irradiated Zn target was dissolved in a few drops of $6N$ HNO_3. Two mg of Ga hold-back carrier (1 mg/ml) and 3 mg of Sb (3 mg/ml) were added. The solution was evaporated to near dryness, cooled, and the residue was transferred with $6N$ HCl solution to a centrifuge tube. H_2S was passed through to precipitate Sb sulfide and coprecipitate the Ge as a sulfide. Sb was chosen as a carrier because of the quick formation of an easily centrifugable sulfide. The Sb-Ge sulfide precipitate was centrifuged, digested with $6N$ H_2S-saturated sulfuric acid, filtered, washed with water and alcohol, and dried. These sources were used for our γ-ray measurements. Immediately after the chemical separation no Ga activities were observed, indicating that this Ge-Sb

† Work supported by the U.S. Atomic Energy Commission.

[1] A. H. W. Aten, Jr., Physica **22**, 288 (1956).

[2] R. A. Ricci and R. Van Lieshout, Nucl. Phys. **10**, 360 (1959).

[3] *Nuclear Data Sheets*, compiled by K. Way *et al.* (Printing and Publishing Office, National Academy of Sciences–National Research Council, Washington, D.C. 20025), NRC 2-341-1959.